JOURNAL OF MECHANICAL ENGINEERING AND SCIENCES
ISSN: 2289-4659 e-ISSN: 2231-8380
VOLUME 20, ISSUE 3, 2026, 12322 - 12335
DOI: https://doi.org/10.15282/jmes.20.3.2026.5.0882

RESEARCH ARTICLE

Battery thermal management system analysis on electric vehicles

N. G. Ping[1], I. A. Ishak[1]*, M. A. R. Azahar[1], M. A. S. A. Aziz[1], M. Arafat[2], F. M. Sakri[3], M. N. F. Kamal[4], N. H. Shaharuddin[5]

[1]Faculty of Engineering Technology, Universiti Tun Hussein Onn Malaysia, Kampus Pagoh, 84600 Johor, Malaysia
[2]Malaysian Institute of Aviation Technology, Universiti Kuala Lumpur, 43900 Sepang, Selangor, Malaysia
[3]Taylor's University, School of Engineering, 1 Jalan Taylor's, 47500 Subang Jaya, Selangor, Malaysia
[4]Pentamaster Corporation, Persiaran Cassia Selatan 6, Taman Perindustrian Batu Kawan, Penang, Malaysia
[5]Department of Mechanical Engineering, Keio University, Yokohama, Japan

Abstract - Battery thermal management systems (BTMS) are crucial for managing the battery temperature in electric vehicles, and their efficiency has become a bottleneck in increasing the charging and discharging rates. This study examines the impact of cell arrangement and coolant type on BTMS performance and identifies the most suitable setup for the current module. ANSYS computational fluid dynamics software was used to simulate the immersion cooling of a battery module containing 96 units of 21700 cylindrical cells. Two cell arrangements and three coolants were simulated at inlet velocities of 0.0020, 0.0045, 0.01, 0.015, and 0.02 m s−1. The inlet velocity was maintained constant at the module inlet, and the pressure loss from the pump was not considered to simplify the study. The results indicate that the aligned module reduced the maximum module temperature and module temperature gradient by 7.91% and 24.64%, respectively. Among the coolants, water exhibited superior cooling performance, reducing the maximum temperature and temperature gradient of the module by 17.61% and 63.77%, respectively. The Analytic Hierarchy Process (AHP) reached the same decision, identifying water as the most suitable alternative for the criteria used in this study. However, water poses a significant safety risk because it can cause a short circuit in the battery when polluted with ions. The study recommends that future work include safety and coolant lifespan as additional AHP criteria and apply more detailed module geometry to achieve more practical results.

Article History
Received : 25 March 2026
Revised : 25 July 2026
Accepted : 3 September 2026
Published : 30 September 2026

Keywords
BTMS
Lithium-ion Batteries
Temperature gradient
Computational fluid dynamics
Analytic hierarchy process
Thermal management

1. Introduction

Electric Vehicles (EVs) and Hybrid Electric Vehicles (HEVs) have gained popularity in recent years owing to their low or zero emissions [1]. Lithium-ion batteries are widely used in EVs as a primary energy source because of their high energy density, low self-discharge rate, and long service life [2]. The battery module dissipates a significant amount of heat during charging and discharging. An increasing charging rate, particularly fast charging, can cause higher heat dissipation [3] – [4]. Lithium-ion batteries are sensitive to temperature and high-temperature fluctuations. To address heat dissipation, EV battery packs are integrated with a Battery Thermal Management System (BTMS). In a battery pack, the smallest unit is a single cell. The cells are linked together to form a module. The modules were then linked to produce a high-voltage battery pack. Figure 1 shows the positions of the cells and modules in a battery pack [5].

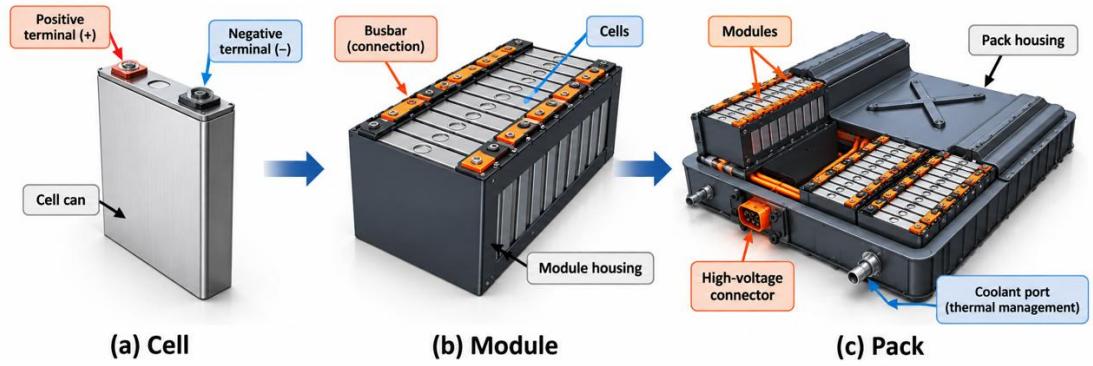


Figure 1. Terms and respective parts of a battery pack (a) cell (b) module (c) pack [5]

The large-scale development of EVs is limited by several critical factors that can cause significant issues in their daily use. For convenience, EVs must improve charging and discharging rates of EVs must be improved to reduce drivers' waiting time at charging stations [5]. In addition, safety is the most important factor in EV development [6]. Currently, thermal runaway in EV battery packs is uncontrollable and poses a critical fire hazard. In addition, battery lifespan is one of the bottlenecks limiting large-scale EV development [7] – [8]. The efficiency of the BTMS determines the maximum charging and discharging rates allowed and the number of battery modules that can be supported by an EV [9– [10]. There are several types of BTMS, including air- and liquid-cooling systems, which are also recognised as active BTMS [11]– [13]. Air-based BTMS have the advantages of a simple structure, low manufacturing cost, and low energy consumption compared with liquid-based BTMS. Nevertheless, large-capacity batteries and fast charging require a higher heat transfer

***CORRESPONDING AUTHOR | I.A. Ishak** | ✉ izuan@uthm.edu.my
© 2026 The Authors. Published by Universiti Malaysia Pahang Al-Sultan Abdullah Press. This is an open access article under the CC BY-NC 4.0 license

coefficient to efficiently remove heat from the battery pack [13] – [14]. Liquid-based BTMS can remove more heat than air-based BTMS in the same volume because they have a higher specific heat capacity [15]. Notably, active BTMS consume electrical energy from the battery, which reduces the EV battery mileage [11]. Thus, it is crucial to study and utilise BTMS to enhance efficiency. A lithium-ion battery has a narrow optimum operating temperature range of 15–35 °C, with a tolerance of 5 °C within a multicell module [16] – [17]. This study focused on the flow structure, mass flow rate, pressure loss, and heat coefficient. As the mass flow rate increases, the pressure loss increases, leading to significant power consumption in the BTMS. A high mass flow rate also increases the risk of BTMS failure, especially coolant leakage, which can cause a circuit shortage within the battery module. Previous studies have focused on optimising air-cooled BTMS via cell arrangement and airflow path design, with limited focus on optimising direct liquid-cooled BTMS. Previous studies have not focused on optimising the parasitic power from the BTMS. Thus, this study was conducted to analyse the impact of cell arrangement on BTMS cooling performance, evaluate the effects of coolant materials on BTMS performance under different velocity values, and determine the suitable configuration of the parameters for the current module.

2. Methods and Material

The following sub-chapters discuss the methods and materials used in this study. The materials used in this study followed the setup described by Moghaddam [18]. The mesh and simulation setup were converted to be compatible with Ansys Fluent, as the original setup was for STAR-CCM+. The simulation study focused on two components: the cooling material and cell arrangement. The final goal was to determine the most efficient BTMS setup for various coolant velocities. To limit the number of variables, battery heat generation was assumed to be a simple, constant heat source. The study was also simplified to be time independent. Temperature colour contours and plotted graphs were prepared to compare the results for each material and cell arrangement. In addition, the AHP was conducted to further analyse the performance of each cooling material based on the preference of each factor.

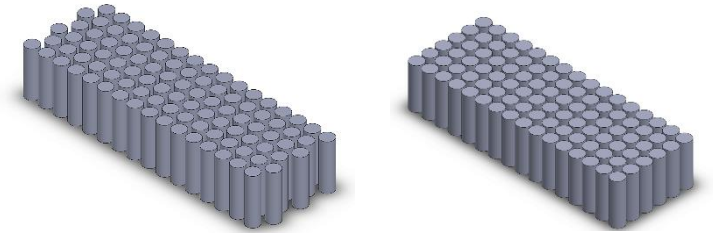
2.1 Materials in the Study

This study focused on analysing a direct liquid-cooled BTMS comprising 96 21700 cylindrical cells, one enclosure, and different coolants. Table 1 lists the properties of the 21700 cells. The dimensions of the 21700 cells can be inferred from their code: “21” represents the cell diameter is 21 mm, “70” represents the cell height is 70 mm, and “0” indicates a cylindrical cell [1], [18]. In this study, we assumed that the heat generation of each cell was constant at 4.4 W. This baseline assumption is informed by empirical heat generation curves from the literature and the practical operating boundaries of electric vehicles (EVs) [18]. For instance, the 2017 Tesla Model 3 adopted 21700 cylindrical cells in its battery pack. According to the manufacturer specifications, 21700 cells are designed to operate continuously between 0.5C and 2.0C on average [19], representing the permissible continuous discharge rate during vehicle operation. The C-rate quantifies the number of times a battery can be fully charged or discharged in one hour. Prior research showed that Novec fluid could control the internal temperature gradient within 5 °C inside a 21700-battery module using dielectric immersion cooling. At this upper cooling boundary, the cell generated 4.4 W of heat at an operating rate of approximately 2.62C. Consequently, this 4.4 W thermal load models a sustainable high-stress scenario, such as high-speed highway cruising or A/C maximum charging operation.

Table 1. 21700 lithium-ion cell properties [41]

Property	Value
Rated discharge capacity (1C-rate)	3.2 Ah
Nominal voltage	3.56 V
Rated discharge energy	11.4 Wh
Density	560 kg m^{-3}
Heat capacity	1000 J kg^{-1} K^{-1}
Radial thermal conductivity	1 W m^{-1} K^{-1}
Axial Thermal conductivity	25 W m^{-1} K^{-1}
Tangential thermal conductivity	25 W m^{-1} K^{-1}
Internal resistance	50 mΩ

The 21700 cells were arranged in two different configurations, as shown in Figure 2. In the first arrangement, the cells were placed in two patterns: three rows were closer to the inlet, and the rest were positioned 12.5 mm behind. In contrast, the aligned cell arrangement spaces the cells equally. Both cell arrangements left a 2 mm gap between the cells. The cells were sealed in a module with walls, one inlet, and one outlet (Figure 3). The flow direction was consistent throughout the simulation for any cell arrangement or any coolant. The enclosure had the same height as the cell, thereby restricting the coolant flow to the cell sidewalls. Table 2 lists the properties of the coolants employed in this study. The coolants were selected based on the common coolants available in the industry. The coolants were applied one type at a time in the simulation with different inlet velocities for comparison.



(a) (b)

Figure 2. Isometric views of the cell configuration for: (a) staggered cell module; (b) aligned cell module

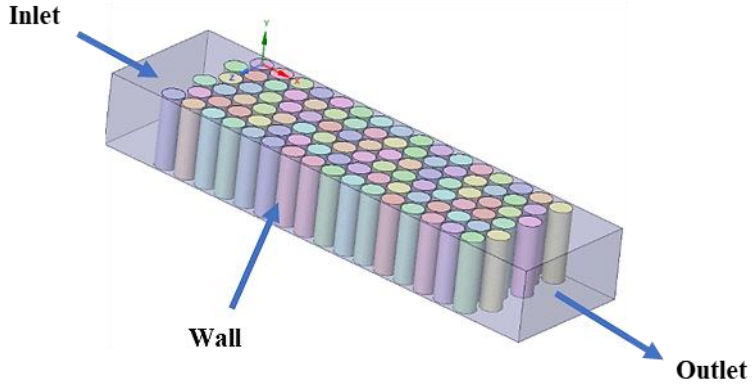


Figure 3. Dimensions of the enclosure

Table 2. Material properties of fluids

Materials	Density ($kg\ m^{-3}$)	Specific heat ($J\ kg^{-1}\ K^{-1}$)	Thermal conductivity ($W\ m^{-1}\ K^{-1}$)	Dynamic viscosity ($Pa{\cdot}s$)
Novec	1660	1130	0.06	0.000870
Ester	804.06	2155	0.1589	0.008290
Water	998.2	4182	0.6	0.0010016

2.2 Mesh independence study

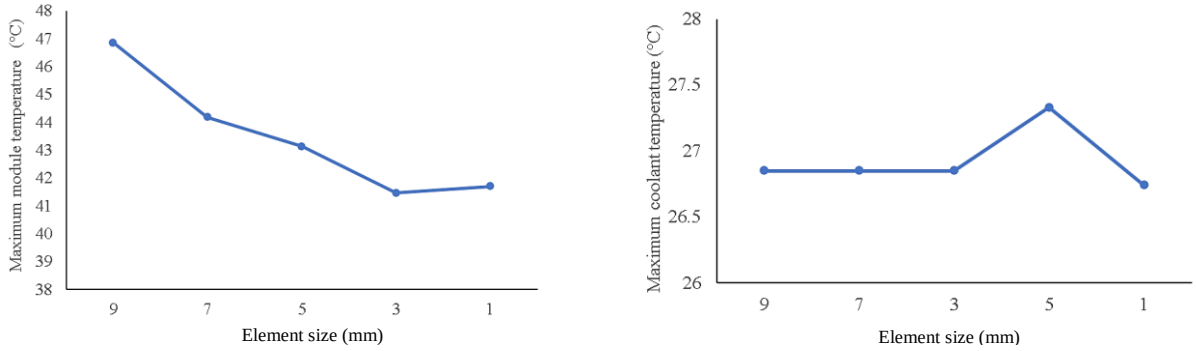
Different mesh element sizes can cause the computational fluid dynamics results to differ, even when the parameter setup remains constant. A finer mesh can lead to more accurate results because it better resolves steep gradients in the flow variables and features. A coarser mesh tends to smooth out important flow features, thereby reducing the result accuracy. Owing to the computational cost, the element size cannot be extremely fine. The element size must be chosen carefully to balance the acceptable computational cost with accurate results. To obtain stable simulation results with a minimum mesh resolution, the simulation parameters were fixed, and the simulation was repeated with different element sizes and temperatures [20]. Table 3 lists the physical parameters used in the simulation and the tested element sizes. The simulation results were compared based on the maximum coolant and module temperature.

Table 3. Parameter setup for the validation test

Parameters	Description
Thermal condition	1 source term, 181400 $W\ m^{-3}$
Inlet velocity	0.0045 $m\ s^{-1}$
Inlet temperature	20°C
Gravity	y-axis, -9.81 $m\ s^{-2}$
Coolant	Novec
Element size	1 mm, 3 mm, 5 mm, 7 mm, 9 mm

Figure 4 shows the results for each element size used. The module temperature decreased significantly with decreasing element size. In contrast, the coolant temperature remained significantly more stable, regardless of the element size. When the element size decreased from 5 to 3 mm, the module temperature dropped from 43.13 to 41.47 °C, a reduction of 3.84%. When the element size was shifted from 3 to 1 mm, the temperature increased from 41.47 to 41.70 °C, a 0.5% increase. In addition, the coolant temperature increased from 26.85 to 27.33 °C and decreased to 26.74 °C when the element size was reduced from 5 to 3 and 1 mm, respectively, indicating that the element size contributed only approximately 2% to the difference in coolant temperature. The results showed that a 3 mm element size is the ideal

option for grid-independent simulations with the lowest computational cost. The graph of the module temperature against the element size also showed that the temperature curve was nearly flat.



(a) (b)

Figure 4. The maximum temperature against mesh size for: (a) the module; (b) the coolant

To verify the results, we compared the simulation with that of a previous study by Moghaddam [18] using an identical module geometry and simulation setup. Figure 5 shows a comparison of the module temperature contours. The comparison confirmed that both contours exhibited an identical pattern, in which the module temperature increased smoothly from the inlet to the outlet. The cells near the outlet had noticeably higher temperatures owing to the turbulent flow. The maximum module temperatures in the previous and current studies were 37.873 °C and 41.47 °C, respectively. The maximum module temperature in the current study was 9.51% higher than that in the previous study. The current study setup was acceptable because the error in the results was controlled to within 10%. This difference could be attributed to the differences in the simulation software and slight differences in the inlet and outlet path lengths.

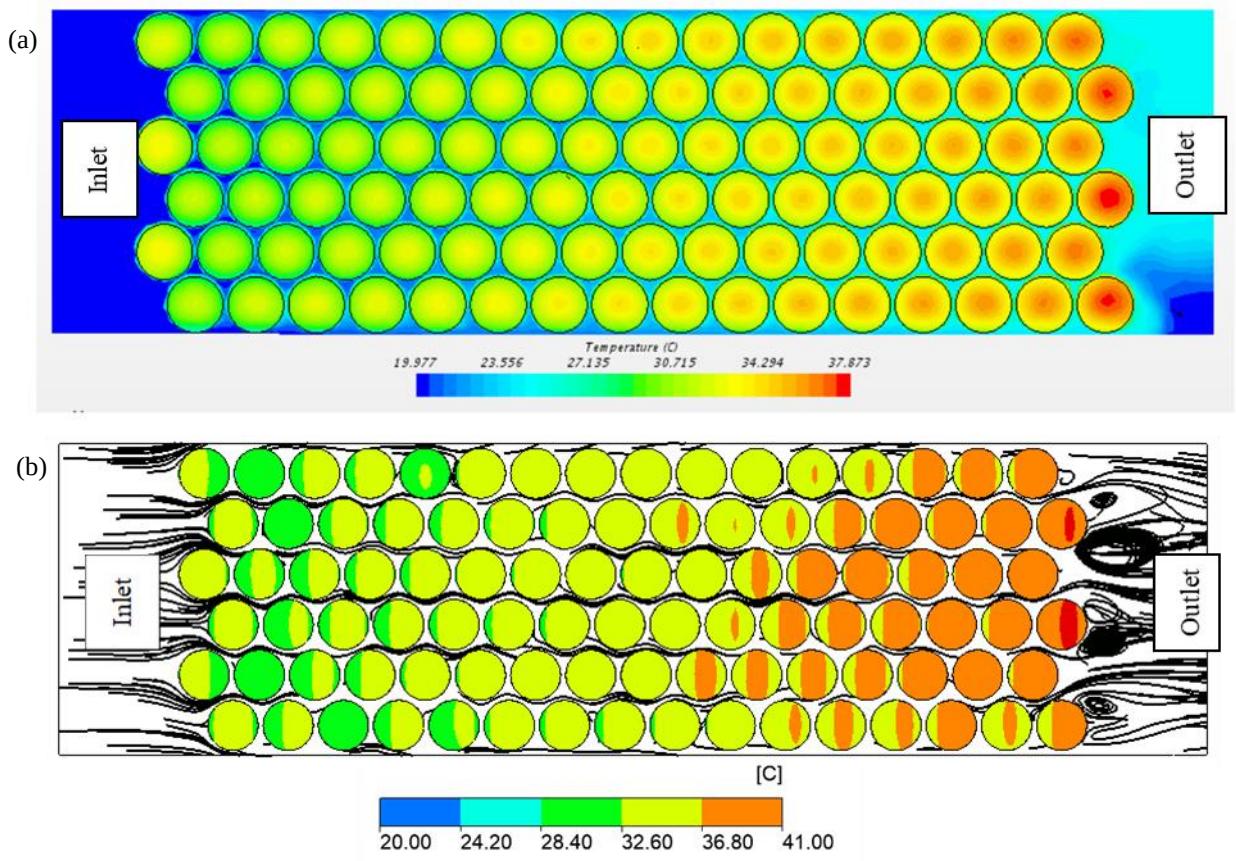


Figure 5. The module temperature contour from: (a) the referred past study [20]; (b) the actual result

In summary, we performed mesh independence and validation studies, as shown in Figure 6. We drew and set up the module and enclosure geometries in the Ansys Workbench Geometry section. We set the mesh to a 9 mm element size at the beginning to allow the simulation to start with minimal computational power. The simulation environment was set to fixed values to allow the module to release heat, and the coolant flowed at a fixed rate over 350 iterations. The coolant and module temperature values and contours were obtained at the end of the simulation. The simulation was repeated by reducing the element size by 2 mm until it reached 1 mm in size. After collecting all the data, the module and coolant temperature curves were plotted against the element size. The largest element size at which the temperature curve flattened

was selected as the grid independence value. The element size was validated using a previous study. If the error was less than 10%, the simulation was accepted; otherwise, the simulation setup was checked and adjusted until the error was reduced to less than 10%.

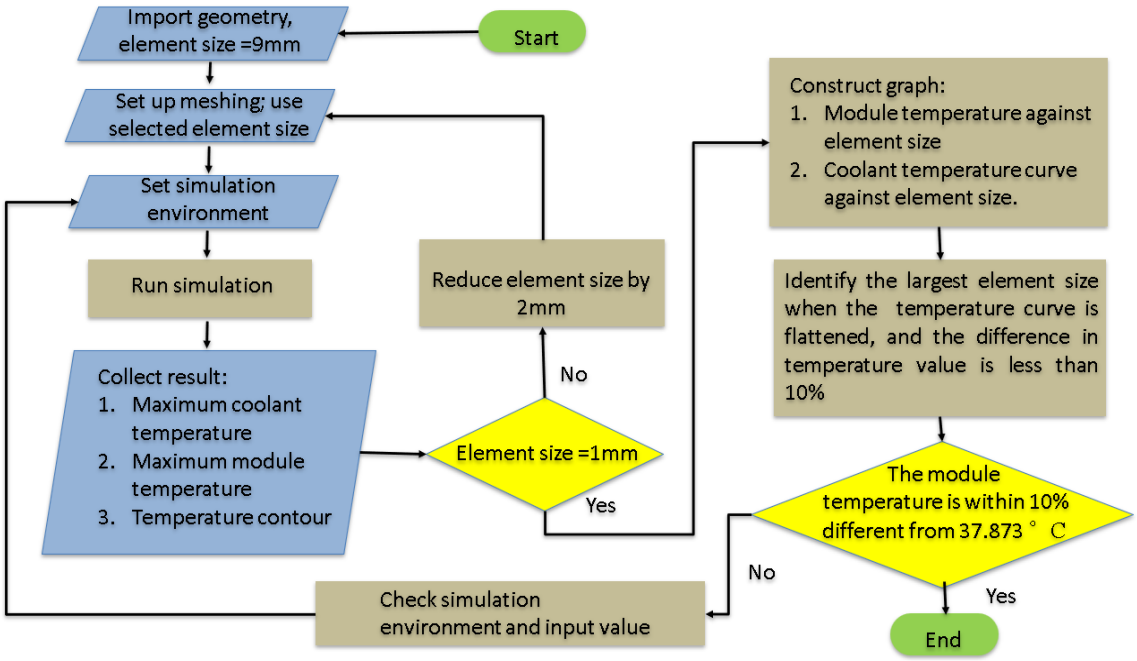


Figure 6. The flow chart used to conduct mesh independence and validation study

The final meshing setup is shown in Figure 7. The mesh element size was set to 3 mm, with 741,072 cells. Multizone was used to configure the mesh setup for the fluid zone (the area excluding the cell) and the cell [21]. An inflation layer was applied to the cylindrical face of the cells to capture the thermal effects near the wall [22]-[23]. The mesh setup was consistently applied across all case studies to ensure accurate results.

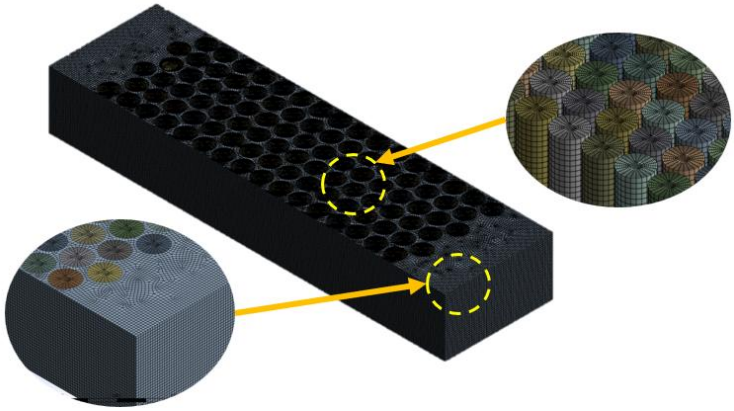


Figure 7. Mesh arrangement of the module

2.3 Methodology

The process of this study is illustrated in Figure 8. The simulation study was initiated after the model passed the mesh independence test. The first aim of the simulation study was to compare the two cell arrangements to acquire the best-performing model. The second simulation study compared the cooling performances of different coolant types. The best-performing model was transferred and applied to a second simulation study. Subsequently, the AHP was conducted to select a suitable coolant in the current module based on the given criteria and goal. After completing the mesh generation, the setup was configured to determine the temperature and pressure distributions within the model. The Reynolds-averaged Navier–Stokes (RANS) methodology was applied to analyse the flow structure inside the model. Table 4 presents the solver configuration. The turbulence effects were modelled using the standard k-epsilon approach with enhanced wall treatment, the RNG model, and a curvature correction set to 1. The energy equation was applied. The Green-Gauss cell-based technique was employed to compute the spatial gradients, enabling a precise representation of the flow field variables [24]. The simulation used internal flow, with the module wall and cylindrical cell surface as the boundaries [25]. In all cases, the heat generation rate remained constant, with each cell releasing 4.4 W. The 350 iterations indicate 350 steps taken throughout the solution process. The iteration number was limited to prevent excessive processing time and ensure that the simulation results converged. Table 4 lists the RANS parameters. Staggered and aligned modules

were applied separately. The first five cases used a staggered cell module, followed by an aligned module. The simulations used 4.4 W of heat generation per cell and five different inlet velocities ranging from 0.002 m s^{-1} to 0.020 m s^{-1}. Table 5 shows the test configuration for the first case study.

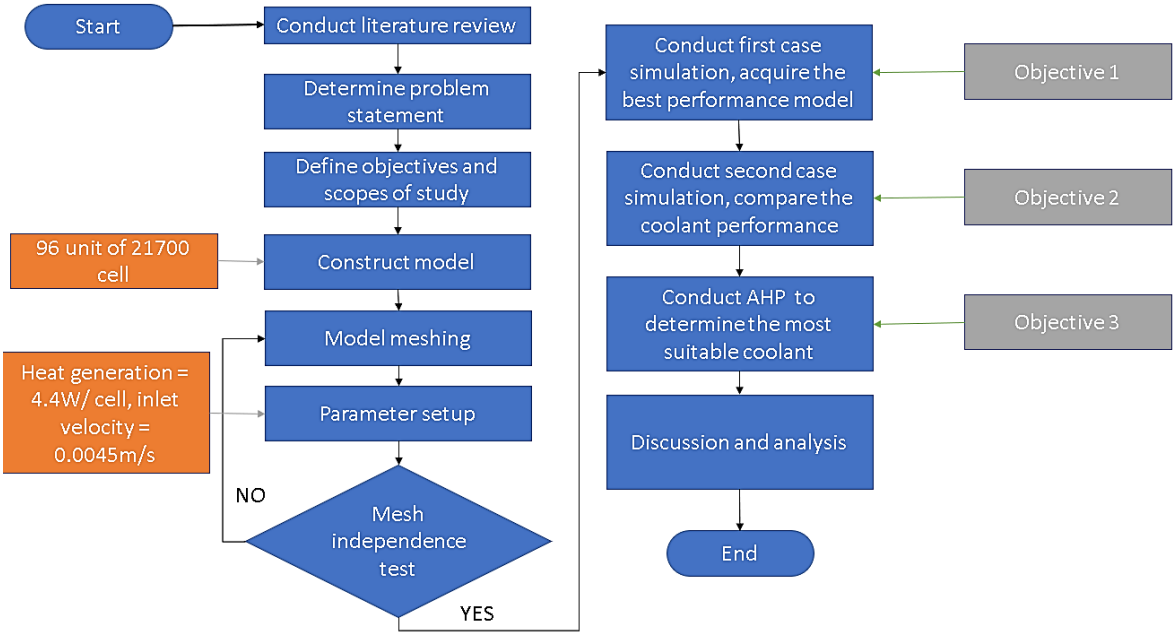


Figure 8. Test configuration

Table 4. Parameters for the RANS approach used in simulation

Parameters	RANS
Model	k-epsilon
Type	Standard
Wall treatment	enhanced wall treatments
Solver type	Steady
Number of iterations	350

Table 5. Test configuration for the second case study

Test number	Module	Heat generation per cell (W)	Inlet velocity (m s^{-1})
1	Staggered	4.4	0.0020
2	Staggered	4.4	0.0045
3	Staggered	4.4	0.0100
4	Staggered	4.4	0.0150
5	Staggered	4.4	0.0200
6	Aligned	4.4	0.0020
7	Aligned	4.4	0.0045
8	Aligned	4.4	0.0100
9	Aligned	4.4	0.0150
10	Aligned	4.4	0.0200

In the second case study, the best-performing module was transferred and applied to the new data. Novec, water, and ester were then used to simulate the BTMS cooling process. In the simulation test, the heat generation was set to 4.4 W per cell, and the inlet velocity was set from 0.0020 m s^{-1} to 0.020 m s^{-1} for each coolant type. Table 6 presents the simulation configuration for each coolant type. After the simulations were conducted, the simulation results were analysed for the coolants. Subsequently, the AHP was conducted based on the simulation results. The AHP was used to determine the most suitable coolant for the current module. To achieve this goal, the coolant was evaluated based on the velocity required to maintain the module temperature below 35 °C, the inlet velocity required to maintain the module temperature gradient within 5 °C, and the coolant pressure drop at 0.02 m s^{-1}. Table 7 lists the AHP components, and Figure 9 shows the AHP hierarchical structure. Figure 10 shows the test rig used in this study. In the simulation, only one module was simulated, which contained 96 cell units. The cell was set to release heat equally at a rate of 181400 W m^{-3}. The pump moved the water in one direction and ensured that the coolant reached the desired velocity at the module inlet. The coolant

entered the module at 20 °C and absorbed the heat from the cells. The radiator removed heat by continuously supplying the module with coolant at a constant temperature of 20 °C.

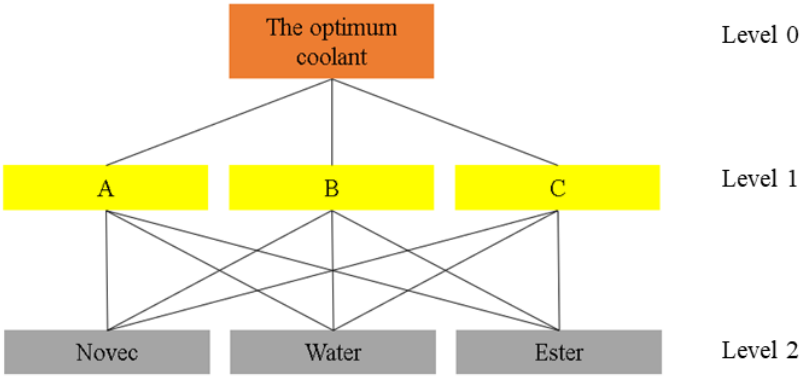


Figure 9. The structure of the hierarchy

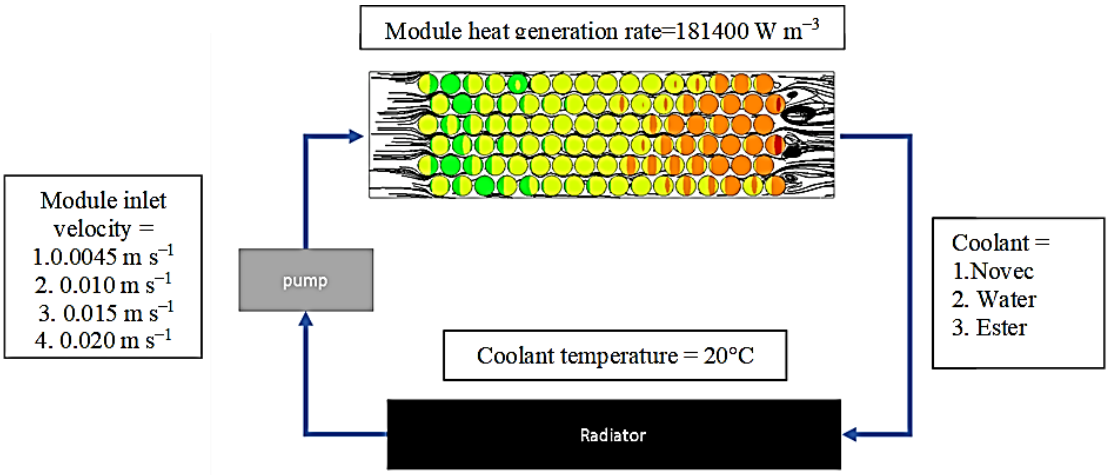


Figure 10. The test rig for the study

Table 6. Test configuration for the second case study

Test number	Coolant	Heat generation per cell (W)	Inlet velocity (m s^{-1})
1	Novec	4.4	0.0020
2	Novec	4.4	0.0045
3	Novec	4.4	0.0100
4	Novec	4.4	0.0150
5	Novec	4.4	0.0200
6	Water	4.4	0.0020
7	Water	4.4	0.0045
8	Water	4.4	0.0100
9	Water	4.4	0.0150
10	Water	4.4	0.0200
11	Ester	4.4	0.0020
12	Ester	4.4	0.0045
13	Ester	4.4	0.0100
14	Ester	4.4	0.0150
15	Ester	4.4	0.0200

Table 7. List of the goal, alternatives, and criteria

Item	Criteria	Definition
Goal	-	The optimum coolant.
Criteria	A	The inlet velocity required to maintain the maximum module temperature is approximately 35°C.
	B	The inlet velocity required to maintain the module temperature gradient within 5°C
	C	The pressure drop of the coolants at maximum inlet velocity (0.02 m s^{-1}).
Alternatives	1	Novec.
	2	Water.
	3	Ester.

3. Result and Discussions

In the following sub-chapters, the simulation results for the impact of cell arrangements and coolant materials on BTMS performance were discussed. The AHP process was then conducted after the result analysis to determine the suitable coolant.

3.1 Impact of Cell Arrangement on BTMS Performance

In the streamlined pattern, the staggered module differed significantly from the aligned module. The streamlines show In the streamlined pattern, the staggered and aligned modules differed significantly. The streamlines show the formation of turbulence in the outlet region of the staggered module. Turbulence formation became dominant as the inlet velocity increased. This was because the coolant flow direction changed randomly within the staggered module. The fluid flowing in random directions interacted with each other in the outlet region and formed a turbulence. Consequently, the formation of turbulence caused poor cooling of the cells adjacent to the outlet. However, the fluid flow pattern remained consistent in the aligned module, regardless of the inlet velocity. This was because of the consistent flow direction within the aligned module. Consequently, the fluid could evenly interact with each cell to absorb heat. In terms of the temperature distribution, the temperature contours for each module exhibited a similar pattern, wherein the cell temperature increased from the inlet and peaked at the outlet. When the inlet velocity was below 0.0150 m s^{-1}, the cells next to the inlet were cooled more effectively in the aligned module than in the staggered module. The difference between the aligned and staggered modules became insignificant when the inlet velocity exceeded 0.0100 m s^{-1}.

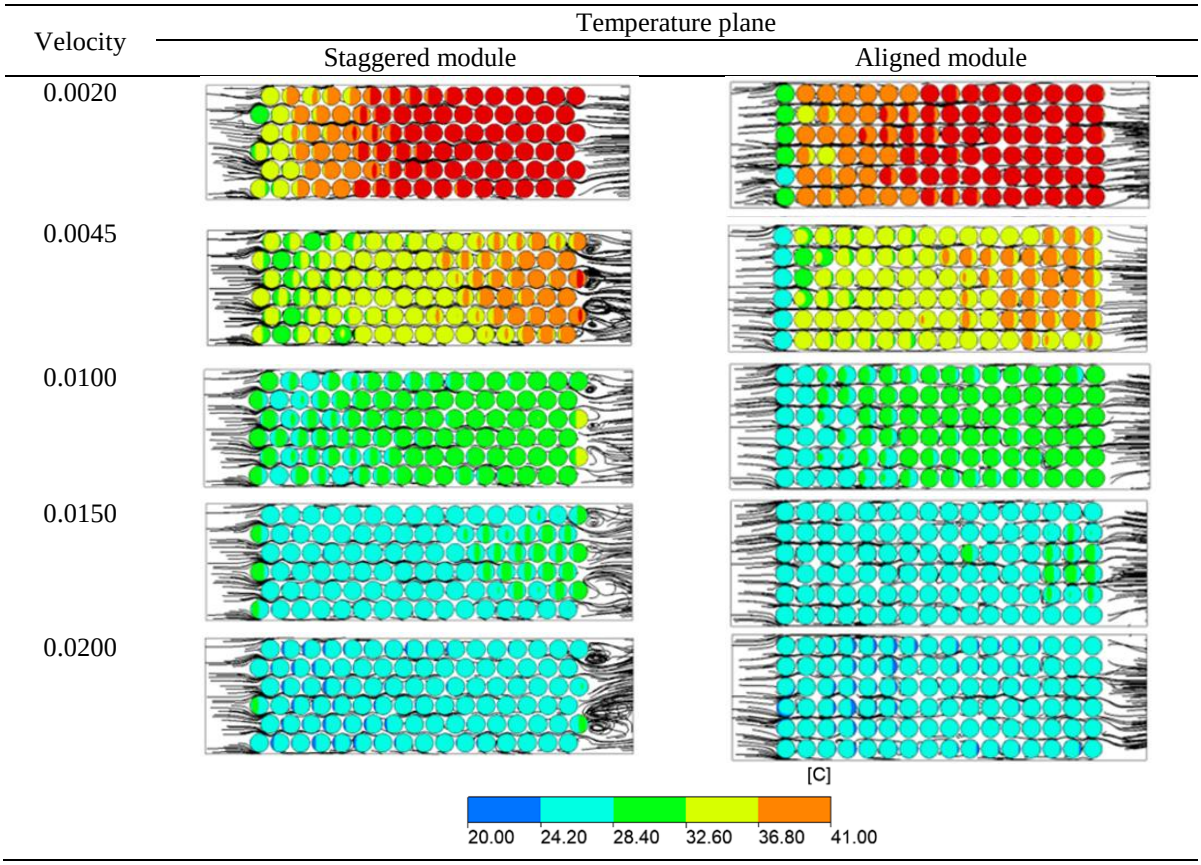


Figure 11. Temperature contour with streamline for the staggered and the aligned module

Figure 11 shows the temperature planes for the aligned and staggered modules from the side view. At 0.0020 m s^{-1}, the staggered module maintained more cells at a lower temperature than the aligned one. However, as the velocity increased to 0.0045 m s-1, the aligned module reduced the temperature gradient to a lower level than that of the staggered module. The temperature contours differed significantly between the two modules in the cells close to the outlet. The cells near the outlet of the staggered module had much higher temperatures due to the formation of turbulent flow. In contrast, the cells in the aligned module exhibited a smooth temperature transition.

Figures 12(a)–(c) compare the performances of the modules. Figure 12(a) shows the maximum module temperature for the two cell arrangements. Each module performed similarly in terms of the maximum module temperature. However, the aligned module maintained a lower maximum module temperature than the staggered module at any velocity. The aligned module maintained a lower maximum coolant temperature starting at 0.0045 m s^{-1}. At the maximum inlet velocity, the aligned module's maximum module and coolant temperatures were 7.91% and 0.74% lower than those of the staggered module, respectively, respectively.

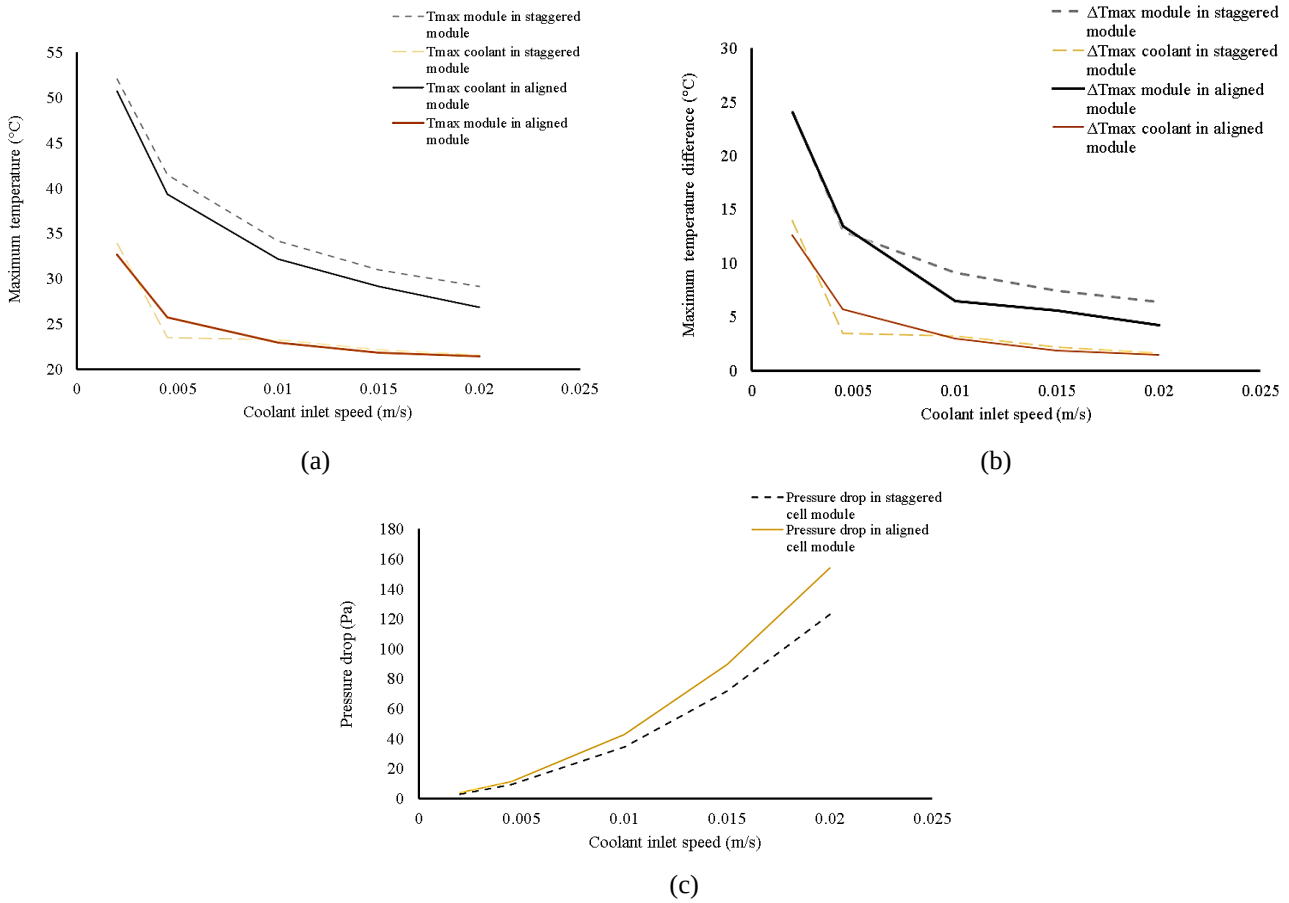


Figure 12. The comparisons of the modules in terms of: (a) maximum temperature; (b) temperature gradient; (c) pressure drop

Figure 12(b) shows the module and coolant temperature gradients for the two cell arrangement types. The coolant temperature showed no significant difference in the same range of coolant velocity. Starting at 0.01 m s^{-1}, the coolant temperature gradient was maintained within ± 5 °C. In terms of the module temperature gradient, the aligned module required a coolant velocity of 0.0020 m s^{-1} to fall below 5 °C, whereas the staggered module could not fall below 5 °C at the maximum coolant velocity. Figure 12(c) shows a graph of the pressure drop against the coolant inlet speed for the two modules. The pressure drops increased with the velocity for both modules. The pressure drop in the aligned module was always higher than that in the staggered module. The pressure-drop difference between the two modules became more significant as the velocity increased. At the maximum velocity, the pressure drop in the aligned module was 25.34% higher than that in the staggered module. This indicated that the aligned module had a lower efficiency than the staggered module, particularly at high inlet velocities. Overall, the study of cell arrangement has shown a similar trait to that of Yang et al., where the cooling efficiency increased when the cells were arranged in an aligned pattern [26]. However, the simulation yielded different findings: the pressure drops increased and the maximum temperature decreased when the cells were arranged in an aligned pattern. This may be because the model used in the previous study had a much shorter flow length and fewer cells. The findings of this study can support the future development of BTMSs for cylindrical cells.

3.2 Impact of coolant material on BTMS performance

The coolant is a key factor in determining the maximum limit of the BTMS [12]. For EVs, the coolant must meet stricter standards. We used Novec, an ester, and water to simulate the BTMS cooling process inside the aligned modules. Figure

13 shows a comparison of the module temperature contours for Novec, ester, and water. In general, the streamline patterns were consistent, regardless of the coolant type or inlet velocity. The streamlines show that the fluid flows smoothly in the gap between each row of cells and exits at the outlet. The cell temperature increased from the inlet and peaked at the outlet. For Novec, the temperature contour showed an inconsistent temperature distribution in the cells at the minimum velocity. This indicates an insufficient coolant flow speed to even the cell temperature. As a result, almost 50% of the cells' temperatures remained above 41 °C, approximately 20% remained between 36.80 and 41 °C, and the rest remained between 20 and 36.80 °C. This uneven temperature distribution can cause serious long-term aging issues. Consequently, the reliability and lifespan of the module decrease. At 0.0100 m s^{-1}, approximately 75% of the cell temperatures remained between 28.40 °C and 32.60 °C, whereas the rest remained between 24.20 °C and 28.40 °C. To maintain all cell temperatures within the same range, the inlet velocity had to be increased to 0.0200 m s^{-1}.

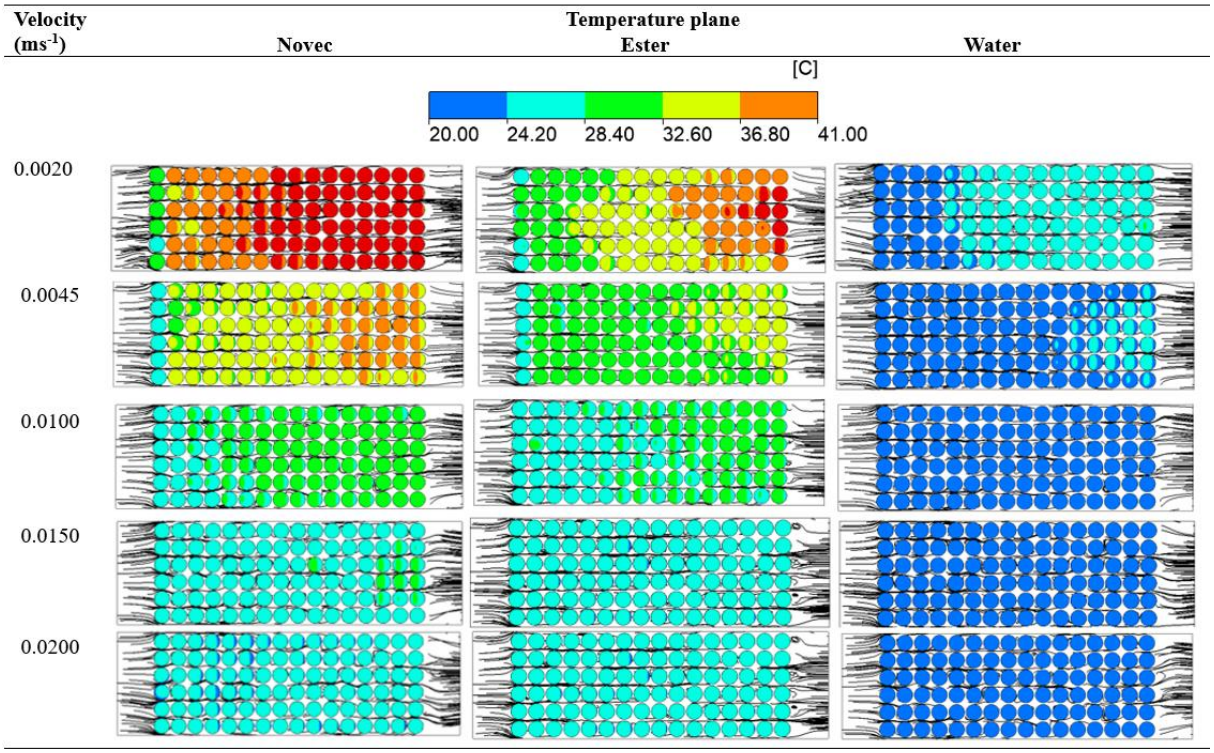


Figure 13. Temperature contour for different types of coolants

For the ester, the temperature contours also showed an uneven temperature distribution in the cells at the minimum velocity. Of the cells, 23.95% had temperatures between 28.40 and 32.60 °C, 41.67% between 32.60 and 36.80 °C, 21.88% between 36.80 and 41 °C, and the remaining cells were below 28.40 or above 41 °C. At low inlet velocities, the ester cannot absorb heat evenly from the cells, leading to uneven aging [17]. The cells near the inlet aged more slowly than those further away from it. At 0.0100 m s^{-1}, approximately 50% of the cell temperatures were between 20.00 °C and 24.20 °C, whereas the rest were between 28.40 °C and 32.60 °C. To maintain all cell temperatures within the same range, the inlet velocity needed to be increased to the maximum value. For water, the cell temperatures were more evenly distributed at the minimum velocity than at the other velocities. In the module, 72.92% of the cells' temperatures ranged between 24.20 and 28.40 °C, whereas the rest ranged between 20.00 and 24.20 °C. Under these conditions, the difference in the aging speed between the cells would be much smaller than that between the ester and Novec. However, the front cells age more slowly than the rear cells, resulting in a shorter module lifespan. To address this issue, the inlet water velocity needed to be increased to at least 0.01 m s^{-1} to keep all the cells within the same temperature range. Regardless of the coolant type, the maximum module temperature decreased as the inlet velocity increased. The maximum module temperature for Novec dropped drastically when the velocity increased from 0.0020 m s^{-1} to 0.01 m s^{-1}. The difference in the module temperature between Novec and the ester decreased as the velocity increased. At 0.0020 m s^{-1}, Novec maintained a lower module temperature than the ester. The module temperature was relatively stable with water. The module temperature became almost constant when the water inlet velocity was set to 0.01 m s^{-1}. At maximum velocity, the module temperature was 17.61% lower when water was used and 4.84% higher when an ester was used compared with Novec. In Figure 14(b), the graph of the module temperature gradient against velocity shows that the temperature gradient decreased regardless of the coolant type. The module temperature gradient for Novec decreased significantly when the velocity increased from 0.0020 m s^{-1} to 0.01 m s^{-1}. Simultaneously, the difference in the temperature gradient between the ester and Novec decreased. Above 0.01 m s^{-1}, Novec reached a lower module temperature gradient than the ester. Water exhibited a relatively smooth and lower temperature curve. At the maximum inlet velocity, the module temperature gradient was 63.77% lower with water and 2.90% higher with ester than that with Novec. In Figure 14(c), the pressure drop for different coolant types is plotted against the velocity. The ester had a significantly higher pressure drop with increasing velocity, followed by Novec and water. The pressure curve for Novec was much closer to that of

water. The difference in the pressure drop between the coolants increased with increasing velocity. At the maximum inlet velocity, the pressure drop was reduced by 34.55% with water and increased by 67.66% with ester compared with Novec. In summary, the findings of this study on coolant materials offer a different perspective from those of the previous study by Moghaddam [18]. Moghaddam [18] compared different types of BTMS. Notably, they used 3M Novec and air in their active cooling BTMS for the same module geometry. In this study, two additional coolant types were added to the simulation to evaluate the impact of the coolant on the BTMS cooling performance. This step was necessary to explore the new possibility of cooling materials in direct liquid cooling BTMS.

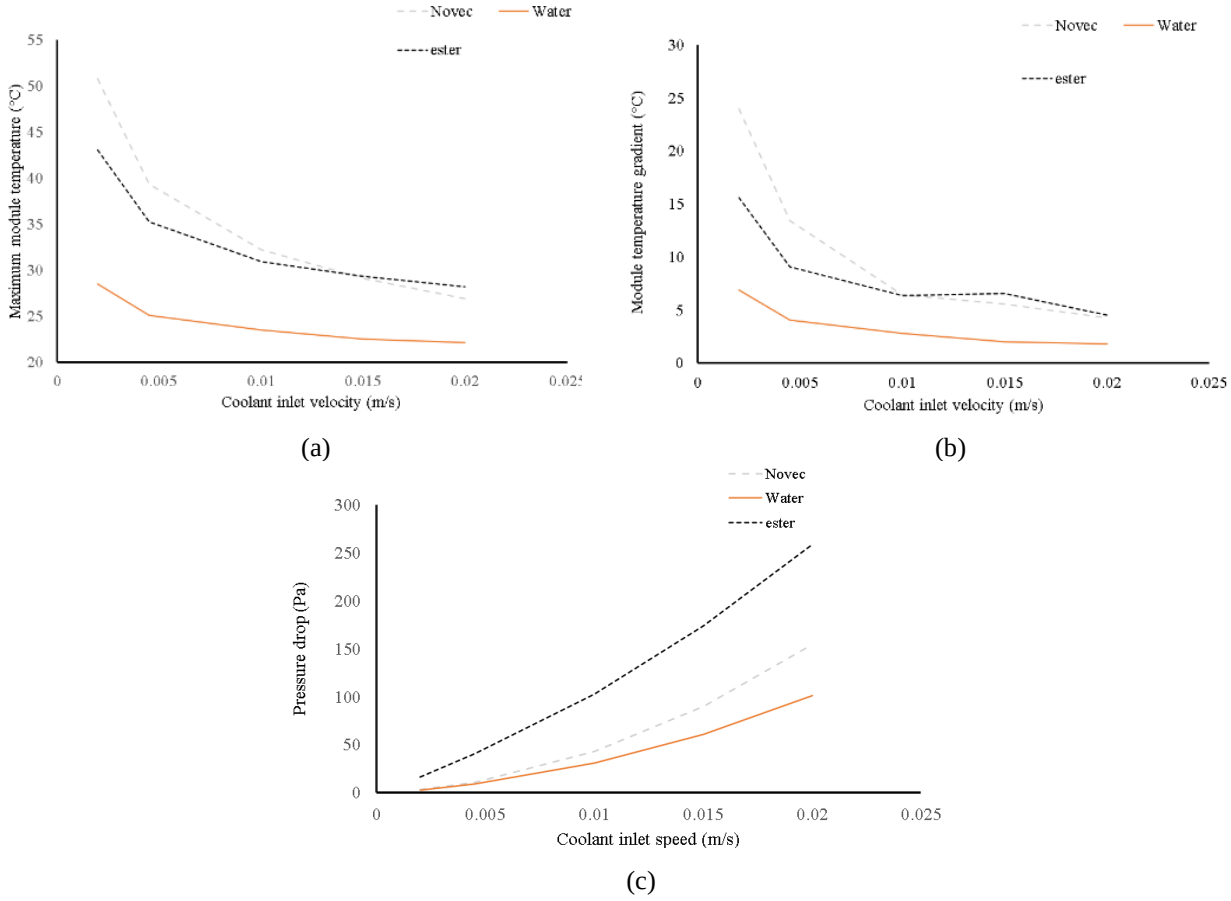


Figure 14. The comparison between coolants in terms of: (a) maximum module temperature against inlet speed; (b) module temperature gradient against inlet speed; (c) pressure drop against inlet speed

3.3 AHP for the coolant

Table 8 presents the comparison matrix for each criterion with respect to the goals. The calculation showed that Criterion B had the largest priority vector, at 58.13%. The second largest criterion was criterion A, which accounted for 30.92% of the priority vector. Criterion C had the smallest priority vector, occupying only 10.96% of the total. The calculated CR value was 0.42%, indicating that the comparison matrix was very consistent. In Table 9, the overall preference of each alternative for the criterion is determined by calculating the total scores. Criterion B had the highest weightage (58.13%), followed by A (30.92%) and C (10.96%). Among the selected criteria, water had the highest score, rated at 43.86% out of 58.13% in criterion B. This indicates that water is an excellent choice when the module temperature gradient is the most important criterion. The ester had the best score for criterion A compared with its scores for criteria B and C. This indicates that the ester has better advantages if the module temperature is maintained below 35 °C was considered more crucial. In contrast, Novec had the best score for criterion C compared with its performance in the other criteria, at 3.39% of 10.96%. This indicates that Novec has a greater advantage in terms of efficiency than maintaining the module temperature below 35 °C or maintaining the temperature gradient. Combining the scores, water scored 71.87% out of 100%, indicating that it was the most optimal alternative when all criteria were considered. Novec had a slightly higher score than the ester, with a total score of 15.61%. The ester accounted for only 12.53% of the total.

Table 8. Paired comparison matrix level 1 with respect to the goal

	A	B	C	Priority vector (%)
A	1	1/2	3	30.92
B	2	1	5	58.13
C	1/3	1/5	1	10.95
Total	10/3	17/10	9	
λ_{max} =3.005, CI = 0.0025, CR = 0.42% < 10% (acceptable)				

In this study, water was the ideal solution for dissipating heat efficiently from the battery pack. However, water can also be hazardous and can severely damage batteries. Pure water does not contain ions that can conduct electricity. However, when water is exposed to carbon dioxide in the air, it reacts to form carbonic acid. In addition, ions from the worn-out metal in the pump can also pollute the deionised water. The presence of ions is difficult to avoid during the operation of immersion-cooled BTMS. An electrical circuit short inside a battery pack can trigger a thermal runaway [1]. In the event of a thermal runaway, water breaks down into hydrogen and oxygen gases. A mixture of heat and flammable gas can trigger an explosion within moments. Thus, the practical use of water in immersion-cooled BTMS is almost non-existent at the current stage of BTMS development. Further improvements in the safety factor are required for water-based immersion-cooled BTMS.

Table 9. Total score of each alternative

Criteria	Criteria Weight (%)	Novec	Water	Ester
A	30.92	3.29	21.64	5.98
B	58.13	8.93	43.86	5.34
C	10.96	3.39	6.37	1.20
Total score (%)		15.61	71.87	12.53

4. Conclusions

In conclusion, this study provides a thorough analysis of the impact of cell arrangement and coolant type on BTMS performance using computational fluid dynamics simulations. The simulations were performed in a steady state, with constant heat generation and varying inlet velocities. The objectives of this study were to analyse the temperature distribution, flow structure, and pressure drop in the modules and coolants, and to identify the effect of cell arrangement and coolant type on BTMS performance. The first objective highlighted how the cell arrangement affects the temperature distribution and pressure drop inside the module and coolant. The results revealed that the aligned module had a more organised flow pattern and better temperature distribution than the staggered module. The second objective showed that different coolant materials significantly affect the BTMS cooling performance. In general, the maximum temperature and temperature gradient for the module and coolant decreased when the inlet velocity increased for all coolants. In contrast, the pressure drops increased with the inlet velocity. The third objective showed that the best configuration for the current BTMS is an aligned module with water as the coolant to achieve optimal performance. We used the MCDA to select the coolant. The AHP method, which is a type of MCDA, provided good insight into coolant evaluation under each criterion. The first-level comparisons between the criteria with respect to the goal showed that the inlet velocity required to maintain the module temperature gradient within 5 °C was the most crucial criterion, occupying 58.13% of the priority vector. Water was the most preferred option under the given criteria. Water scored 71.87% overall, whereas Novec and the ester scored 15.61% and 12.53%, respectively. The CR value for all pairwise matrices was below 10%, indicating that the AHP was consistent and the decision to select the water source was reliable.

The current study assumed a perfect operating environment for the BTMS and did not consider the risk of system leakage or coolant lifespan. The current study used only simplified cell, inlet, and outlet geometries in the simulation. Future studies should consider coolant safety and lifespan in AHP to obtain more practical decision-making results. In terms of geometry, future studies should use more detailed component geometries to obtain more accurate results. The current study is also limited to a steady environment, where the battery SoC is constant and produces a constant heat output into the coolant. This assumption does not fully cover the battery operating conditions under different loads and SoC. Thus, future studies should consider the battery pack behaviour under different operating conditions to obtain more precise results.

Acknowledgements

The authors thank Universiti Tun Hussein Onn Malaysia (UTHM) for providing facilities and funding for this study

Funding

This work was supported by Universiti Tun Hussein Onn Malaysia through a Tier 1 grant (vot Q939).

Conflict of Interest

The authors declare no conflicts of interest.

CRediT Author Contribution Statement

N. G. Ping: Methodology; Analysis; Investigation; Data curation; Writing-original draft
I. A. Ishak: Conceptualisation; Supervision; Writing – review & revise
M. A. R. Azahar: Methodology; Writing – review & revise
M. A. S. A. Aziz: Methodology; Writing – review & revise
M. Arafat: Conceptualisation; Methodology; Writing – review & revise
F. M. Sakri: Analysis; Visualisation; Writing – review & revise
M. N. F. Kamal: Analysis; Validation; Writing – review & revise
N. H. Shaharuddin: Investigation; Writing – review & revise

Availability of Data and Materials

The datasets generated and/or analysed during the current study are available from the corresponding author upon reasonable requests.

Ethics Declarations

This study did not involve human participants or animal subjects. Therefore, ethical approval was not required for this study.

Generative Artificial Intelligence Declarations

The authors claim that artificial intelligence-assisted technologies, such as generative AI, were not used to generate content, ideas, or theories. We used AI to enhance the readability and refine the language. This was performed with extreme human control and oversight. The authors take full responsibility for reviewing and approving the content.

References

[1] G. Guo, B. Long, B. Cheng, S. Zhou, P. Xu, and B. Cao, "Three-dimensional thermal finite element modeling of lithium-ion battery in thermal abuse application," *Journal of Power Sources*, vol. 195, no. 8, pp. 2393–2398, 2010, https://doi.org/10.1016/j.jpowsour.2009.10.090.

[2] A. A. Pesaran, S. Burch, and M. Keyser, "An approach for designing thermal management systems for electric and hybrid vehicle battery packs," National Renewable Energy Laboratory, Golden, CO, USA, Rep. NREL/CP-540-25992, 1999. Presented at the 4th Vehicle Thermal Management Systems Conf., London, U.K., May 24–27, 1999.

[3] Y. Zeng, D. Chalise, S. D. Lubner, S. Kaur, and R. S. Prasher, "A review of thermal physics and management inside lithium-ion batteries for high energy density and fast charging," *Energy Storage Materials*, vol. 41, pp. 264–288, 2021, https://doi.org/10.1016/j.ensm.2021.06.008.

[4] A. Tomaszewska, Z Chu, X Feng et al., "Lithium-ion battery fast charging: A review," *eTransportation*, vol. 1, Art. no. 100011, 2019, https://doi.org/10.1016/j.etran.2019.100011.

[5] A. Thaler and D. Watzenig, *Automotive Battery Technology* (SpringerBriefs in Applied Sciences and Technology). Cham, Switzerland: Springer; 2014. pp. 1–129, https://doi.org/10.1007/978-3-319-02523-0.

[6] M. J. Uddin, M. M. H. Mia, M. O. Faruk, R. Hasan, and M. Miya, "Developments, obstacles, and opportunities in electric vehicle (EV) powertrain and battery technologies," *Scientia: Technology, Science and Society*, vol. 2, no. 9, pp. 65–74, 2025, https://doi.org/10.59324/stss.2025.2(9).07.

[7] H. Roy, B. N. Roy, M. Hasanuzzaman et al., "Global advancements and current challenges of electric vehicle batteries and their prospects: A comprehensive review," *Sustainability*, vol. 14, no. 24, Art. no. 16684, 2022, https://doi.org/10.3390/su142416684.

[8] X. Sun, Z. Li, X. Wang, and C. Li, "Technology development of electric vehicles: A review," *Energies*, vol. 13, no. 1, Art. no. 90, 2019, https://doi.org/10.3390/en13010090.

[9] P. Zare, N. Perera, J. Lahr, and R. Hasan, "A novel thermal management system for cylindrical lithium-ion batteries using internal-external fin-enhanced phase change material," *Applied Thermal Engineering*, vol. 238, Art. no. 121985, 2024, https://doi.org/10.1016/j.applthermaleng.2023.121985.

[10] D. Luo, Z. Wu, Y. Yan et al., "Performance investigation and design optimization of a battery thermal management system with thermoelectric coolers and phase change materials," *Journal of Cleaner Production*, vol. 434, Art. no. 139834, 2024, https://doi.org/10.1016/j.jclepro.2023.139834.

[11] M. A. Rahman, G. M. V. Reddy, R. Chatterjee et al., "Energy sources and thermal management technologies for electric vehicle batteries: A technical review," *Global Challenges*, vol. 9, no. 7, Art. no. e2500083, 2025, https://doi.org/10.1002/gch2.202500083.

[12] T. I. C. Buidin and F. Mariasiu, "Battery thermal management systems: Current status and design approach of cooling technologies," *Energies*, vol. 14, no. 16, Art. no. 4879, 2021, https://doi.org/10.3390/en14164879.

[13] J. Lin, X. Liu, S. Li, C. Zhang, and S. Yang, "A review on recent progress, challenges and perspective of battery thermal management system," *International Journal of Heat and Mass Transfer*, vol. 167, Art. no. 120834, 2021, https://doi.org/10.1016/j.ijheatmasstransfer.2020.120834.

[14] A. R. Abdullah, L. Hongkun, M. M. Noor, H. Santhanam, and K. Kadirgama, "A comprehensive systematic review of the cooling technique for battery thermal management systems in electric vehicles," *Journal of Advanced Vehicle System*, vol. 16, no. 1, pp. 23–49, 2025, https://doi.org/10.37934/javs.16.1.2349.

[15] T. Han, B. Khalighi, E. C. Yen, and S. Kaushik, "Li-ion battery pack thermal management: Liquid versus air cooling," *Journal of Thermal Science and Engineering Applications*, vol. 11, no. 2, Art. no. 021009, 2019, https://doi.org/10.1115/1.4041595.

[16] J. Wang, Q. Zheng, M. Fang, S. Ko, Y. Yamada, and A. Yamada, "Concentrated electrolytes widen the operating temperature range of lithium-ion batteries," *Advanced Science*, vol. 8, no. 18, Art. no. 2101646, 2021, https://doi.org/10.1002/advs.202101646.

[17] S. Lv, X. Wang, W. Lu, J. Zhang, and H. Ni, "The influence of temperature on the capacity of lithium ion batteries with different anodes," *Energies*, vol. 15, no. 1, Art. no. 60, 2021, https://doi.org/10.3390/en15010060.

[18] S. M. Hosseini Moghaddam, "Designing battery thermal management systems (BTMS) for cylindrical lithium-ion battery modules using CFD," M.S. thesis, KTH Royal Inst. of Technology, Stockholm, Sweden, 2018.

[19] S. Kocsis Szürke, G. Á. Gladics, and I. Lőrincz, "Analysis of the relationship between discharge cutoff voltage and thermal behavior in different lithium-ion cell types," *Applied Sciences*, vol. 16, no. 1, Art. no. 79, 2025, https://doi.org/10.3390/app16010079.

[20] M. A. S. Abdul Aziz, N. Darlis, I. A. Ishak, N. A. Zolpakar, M. Arafat, and M. M. Muhammadu, "Thermal performance improvement of microchannel heat sink for electronic device cooling system using numerical analysis," *Journal of Advanced Research in Numerical Heat Transfer*, vol. 26, no. 1, pp. 84–98, 2024, https://doi.org/10.37934/arnht.26.1.8498.

[21] Y.-H. Lin and X.-C. Li, "The investigation of a sliding mesh model for hydrodynamic analysis of a SUBOFF model in turbulent flow fields," *Journal of Marine Science and Engineering*, vol. 8, no. 10, Art. no. 744, 2020, https://doi.org/10.3390/jmse8100744.

[22] A. Ahsan and D. Banuri, "CFD-based analysis of divergent section deflection for thrust vector control in 2D nozzles," *Acceleron Aerospace Journal*, vol. 5, no. 1, pp. 1281–1295, 2025, https://doi.org/10.61359/11.2106-2542.

[23] Q. Yang *et al.*, "RANS-based modelling of turbulent flow in submarine pipe bends: Effect of computational mesh and turbulence modelling," *Journal of Marine Science and Engineering*, vol. 11, no. 2, Art. no. 336, 2023, https://doi.org/10.3390/jmse11020336.

[24] W. C. Lim, I. Amin Ishak, M. Arafat, M. Nabil Farhan Kamal, N. Afzanizam Samiran, and A. Faiz Mohammad, "Analysis of the aerodynamic characteristics of small-sized car vehicles under the influence of steady crosswind," *International Journal of Application on Sciences, Technology and Engineering*, vol. 1, no. 1, pp. 217–224, 2023, https://doi.org/10.24912/ijaste.v1.i1.217-224.

[25] M. H. Mohammad Aris, N. Darlis, I. A. Ishak, S. Sulaiman, N. Jaat, and A. F. Hakim, "HVAC CFD analysis of air flow and temperature distribution inside passenger compartment," *Journal of Automotive Powertrain and Transportation Technology*, vol. 1, no. 1, Art. no. 003, 2021, https://doi.org/10.30880/japtt.2021.01.01.003.

[26] N. Yang, X. Zhang, G. Li, and D. Hua, "Assessment of the forced air-cooling performance for cylindrical lithium-ion battery packs: A comparative analysis between aligned and staggered cell arrangements," *Applied Thermal Engineering*, vol. 80, pp. 55–65, 2015, https://doi.org/10.1016/j.applthermaleng.2015.01.049.